Elements of comparison between Martian and terrestrial mesoscale meteorological phenomena: Katabatic winds and boundary layer convection

A. Spiga *,[1]

Department of Physics and Astronomy, The Open University, Walton Hall, Milton Keynes, MK7 6AA, UK

A B S T R A C T

Terrestrial and Martian atmospheres are both characterised by a large variety of mesoscale meteorological events, occurring at horizontal scales of hundreds of kilometres and below. Available measurements from space exploration and recently developed high-resolution numerical tools have given insights into Martian mesoscale phenomena, as well as similarities and differences with their terrestrial counterparts. The remarkable intensity of Martian mesoscale events compared to terrestrial phenomena mainly results from low density and strong radiative control. This is exemplified in the present paper by discussing two mesoscale phenomena encountered in the lowest atmospheric levels of both planets with notable differences: nighttime katabatic winds (drainage flow down sloping terrains) and daytime boundary layer convection (vertical growth of mixed layer over heated surfaces). While observations of katabatic events are difficult on Earth, except over vast ice sheets, intense clear-cut downslope circulations are expected to be widespread on Mars. Convective motions in the daytime Martian boundary layer are primarily driven by radiative contributions, usually negligible on Earth where sensible heat flux dominates, and exhibit turbulent variances one order of magnitude larger. Martian maximum heat fluxes are not attained close to the surface as on Earth but a few hundreds of metres above, which implies generalised definitions for mixing layer scales such as vertical velocity w_*. Measurements on Mars of winds in uneven topographical areas and of heat fluxes over flat terrains could be useful to assess general principles of mesoscale meteorology applicable to both terrestrial and Martian environments.

1. Introduction

Mesoscale meteorology deals with atmospheric phenomena occurring at horizontal scales of hundreds of kilometers and below.[2] A rich zoo of terrestrial meteorological phenomena, part of which can be experienced in everyday life, falls into this category (Orlanski, 1975). This is illustrated, for instance, by the variety of terrestrial clouds: cumulonimbus as a result of deep moist convection, lenticular clouds as a result of flow/topography interactions, cumulus streets as a result of boundary layer convection, et cetera.

The first comprehensive mesoscale studies were often motivated by concerns about meteorological hazards at regional scales. In the 1970s, numerical models were employed to complement earlier investigations based on theoretical consid-

erations and remote-sensing or in situ data analysis. Japanese and American meteorologists discussed the theory of tropical hurricanes (Yanai, 1961) before realistic simulations could be achieved (Anthes et al., 1971). Seminal theoretical work by Kolmogorov and Batchelor on small-scale turbulence in the 1960s (see Fedorovich et al., 2004 for a historical perspective) was followed by high-resolution modeling in the practical case of the boundary layer convection (Lilly, 1962). Numerical models of atmospheric flow impinging a topographical obstacle became more sophisticated (Mahrer and Pielke, 1977), so as to interpret new datasets acquired by aircraft measurements (Lilly and Kennedy, 1973).

In the 1980s and beyond, a more unified approach was adopted. The modeling efforts were pursued to build platforms capable of reproducing the mesoscale variability in any region of the world at various horizontal scales (Pielke et al., 1992). Those efforts yield the versatile three-dimensional mesoscale models used nowadays (Skamarock and Klemp, 2008) in operational weather prediction, meteorological research and, as for the present paper, planetary science studies.

Exploration of the Martian environment provided new perspectives for mesoscale meteorology studies. An important milestone was the Viking missions in the end of the 1970s. In situ

---

measurements (Hess et al., 1977; Sutton et al., 1978), later complemented by the Pathfinder (Schofield et al., 1997) and Phoenix (Davy et al., 2010) missions, showed large diurnal variations of Martian winds and atmospheric stability in the boundary layer. Satellite imagery revealed convective clouds, dust devils (Thomas and Gierasch, 1985) and lee waves (Pickersgill and Hunt, 1979). In the late 1990s and early 2000s, Martian mesoscale phenomena were extensively observed through the instruments on board the Mars Global Surveyor mission: frontal dust storms (Wang et al., 2003), spiral dust clouds (Rafkin et al., 2002), dust devils (Malin and Edgett, 2001), gravity waves (Creasey et al., 2006), "aster" water ice clouds (Wang and Ingersoll, 2002). Further diagnostics of the Martian dust storms, boundary layer phenomena, gravity waves have been obtained from the most recent missions too: Mars Exploration Rovers (Smith et al., 2006), Mars Express (Spiga et al., 2007; Stanzel et al., 2008], Mars Reconnaissance Orbiter (Malin et al., 2008) and Mars Phoenix Lander (Whiteway et al., 2009).

Such a context of observational achievements and availability of flexible terrestrial regional climate models motivated the development of dedicated mesoscale models for the Martian atmosphere (Rafkin et al., 2001; Tyler et al., 2002; Toigo and Richardson, 2002; Spiga and Forget, 2009), which relied on state-of-the-art physical parameterisations of dust, CO_2 and H_2O cycles in Martian General Circulation Models (e.g. Forget et al., 1999). Martian mesoscale models proved to be powerful tools to complement the preliminary work performed with idealised models to characterise the mesoscale variability in the Martian atmosphere (Ye et al., 1990; Haberle et al., 1993a, b; Savijärvi et al., 2004). Notable progress was achieved in understanding convection in the boundary layer (Toigo et al., 2003; Michaels and Rafkin, 2004; Richardson et al., 2007; Spiga et al., 2010), slope circulation (Tyler et al., 2002; Michaels et al., 2006; Spiga and Forget, 2009), dynamics in polar regions (Toigo and Richardson, 2002; Tyler and Barnes, 2005; Kauhanen et al., 2008), atmospheric hazards at selected landing sites (Rafkin and Michaels, 2003; Tyler et al., 2008). Those studies showed how intense the mesoscale circulation is on Mars and discussed the influence of the Martian high thermal contrasts, short radiative timescales, low atmospheric density and steep topographical gradients.

The mesoscale variability of the extreme Martian environment expands the knowledge of mesoscale phenomena on Earth. The present paper is not aimed at giving a detailed review of this Martian mesoscale variability and the contrasts with its terrestrial counterpart, but focuses on two near-surface mesoscale phenomena encountered in both planets with notable differences: night-time katabatic winds and daytime boundary layer convection. The paper consists of a new presentation of results established in previous studies, including the most recent ones,[3] rather than a report of original results in itself. The comparative planetology approach adopted in this paper is thought to give insights into the general principles governing the mesoscale meteorology processes.

2. Katabatic winds

2.1. General principles

Katabatic winds are drainage atmospheric flows that form when cooled dense air is accelerated down sloping terrains by
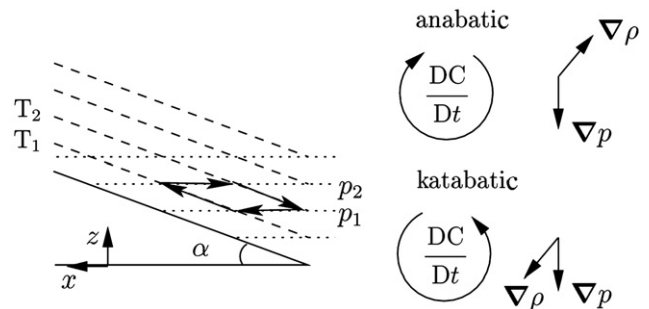
Fig. 1. Basic principle of katabatic (and anabatic) winds. On the left, inclination of isotherms over sloping terrains in situation of nighttime radiative cooling is shown. For the sake of simplicity, pressure is the chosen vertical coordinate. On the right, orientation of circulation's intensification is given according to the baroclinic production (Bjerknes theorem). Nocturnal temperature inversion causes downslope orientation of the winds. Arrows indicate the contour used to calculate the "slope-buoyancy" term (see text). The two isotherms T_1 and T_2 are assumed to be spaced so that $\Delta T = T_1 - T_2$ yields a realistic estimate of the near-surface temperature inversion.

gravity, overcoming the opposing along-slope pressure gradient (Mahrt, 1982). Nighttime terrestrial and Martian conditions are conducive to this behaviour owing to radiative cooling of surface and atmosphere. Atmospheric temperature (thus density) near the ground departs from the reference vertical stratification and adopts a terrain-following behaviour from which originates the katabatic circulation.

Katabatic winds are not theoretically different from thermally induced winds such as sea/land breezes. They can be described as circulation patterns[4] $C = \oint \mathbf{v} \cdot d\mathbf{s}$ obeying the Bjerknes theorem

$$\frac{dC}{dt} = \iint \frac{1}{\rho^2} (\boldsymbol{\nabla}\rho \wedge \boldsymbol{\nabla}p) \cdot d\mathbf{S} \tag{1}$$

Near-surface tilting of the density gradient $\boldsymbol{\nabla}\rho$ with respect to the pressure gradient $\boldsymbol{\nabla}p$ causes baroclinic production $\boldsymbol{\nabla}\rho \wedge \boldsymbol{\nabla}p$ and intensification of wind circulation C (Thorpe et al., 2003). In other words, conversion of (available) potential energy into kinetic energy gives birth to the along-slope circulation. As shown in Fig. 1, in nighttime conditions, orientation of density gradient $\boldsymbol{\nabla}\rho$ is constrained by the near-surface temperature inversion resulting from radiative cooling, hence the downslope (katabatic) character of the winds.[5]

It could be shown, using the contour displayed in Fig. 1, that integration of the Bjerknes formula yields a frictionless upper limit value for the acceleration of the wind along a slope of inclination α

$$\Gamma = \frac{g \sin\alpha \Delta T}{\langle T \rangle} \tag{2}$$

where ΔT is the near-surface temperature inversion, $\langle T \rangle$ is the average near-surface temperature and g is the acceleration of gravity. Γ is sometimes called the "slope-buoyancy" (Parish, 2003) and shows that katabatic wind acceleration varies with slope inclination and near-surface temperature inversion, but not with slope length.

Realistic quantitative estimates of katabatic winds cannot be obtained by retaining the "slope-buoyancy" term only, in what

---

[3] As far as Martian numerical simulations are concerned, results from the Spiga and Forget (2009) mesoscale model are described in greater detail, although references to independent simulations are also given.

[4] $\mathbf{v}$ is the wind velocity and $\mathbf{s}$ is an infinitesimal element of a given closed chain of fluid particles. $\mathbf{S}$ is the equivalent for the surface enclosed within the closed chain of fluid particles.

[5] Note that afternoon anabatic (upslope) winds are explained by the reverse situation of positive buoyancy where the sun-heated surface is warmer than the atmosphere above. A more elaborate analogy than the Bjerknes theorem for anabatic winds is the heat engine theory for convective circulations (Souza et al., 2000), where effects of friction can be easily included.

Mahrt (1982) named a simple advection-gravity equilibrium. The influence of frictional effects, neglected in the derivation of the Bjerknes theorem in Eq. (1), has to be considered. The "slope-buoyancy" term together with the turbulent and adiabatic terms leads to the simple Prandtl analytic slope wind model, which enables one to get plausible first-order estimates of observed steady-state katabatic winds on Mars (Savijärvi and Siili, 1993) and on the Earth (Parmhed et al., 2004).

2.2. Terrestrial examples

The climatology, development mechanisms and regional particularities of terrestrial katabatic winds have been abundantly discussed in the literature (e.g. Manins and Sawford, 1979; Papadopoulos and Helmis, 1999) with particular emphasis on their influence on rainfall rates and concentration of pollutants. Extensive measurement campaigns were carried out in the 1980s–1990s (Horst and Doran, 1986; Mahrt and Larsen, 1990) to complement the earlier theoretical efforts (Mahrt, 1982).

Clear-cut katabatic events are usually not observed in overcast conditions that reduce the outgoing longwave radiation (Drobinski et al., 2003). Another key factor to observe katabatic circulation on Earth is a relative weakness of ambient winds (Horst and Doran, 1986), so that the "slope-buoyancy" force dominates the large-scale pressure gradient force. On gentle slopes with developed upslope winds, observations by Mahrt and Larsen (1990) showed that only very stable conditions could ensure the existence of katabatic winds, which was confirmed by numerical modeling (Skyllingstad, 2003). In many cases, even above steeper slopes, the downslope acceleration of near-surface cold air is adversely affected by mixing with ambient flow, especially when the turbulence is strong (Manins and Sawford, 1979). A notable example was described by Whiteman et al. (1999): the nighttime evolution of the Grand Canyon thermal structure toward weak stability conditions contrasts with other Rocky Mountain valleys (where strong nocturnal inversions develop) and results in infrequent katabatic events despite steep canyon slopes.

The presence of snow or ice on the surface usually leads to more intense and persistent katabatic events. For instance in Rocky Mountains valleys, nighttime temperature inversions are strongest in winter during clear undisturbed nights when snow cover is present, because of weak upward sensible heat fluxes and strong net longwave radiation losses (Doran et al., 1990). In conditions of wintertime permanent snow cover, downslope winds persist over the whole day. Unsurprisingly, the most distinctive terrestrial katabatic winds occur over the ice-covered Greenland and Antarctic continents, where the near-surface temperature inversions in winter reach 25 K (Parish and Waight, 1987; Bromwich et al., 2001). Amplitudes of the winds over the continent reach $10-15\,\mathrm{m\,s^{-1}}$ a few tens of metres above the ground (to be compared to typical mean values of $5\,\mathrm{m\,s^{-1}}$ for katabatic events outside polar regions) but are frequently doubled (see Fig. 2) close to the steep-sloped coastal boundaries (Parish and Waight, 1987). In the Antarctic McMurdo dry valleys, observed katabatic wind speeds are typically $20\,\mathrm{m\,s^{-1}}$ with gusts exceeding $35\,\mathrm{m\,s^{-1}}$, so strong the induced compressional warming increases air temperature by 30 K (Nylen et al., 2004). Abrupt variations of slope can also cause non-linear phenomena such as hydraulic jumps at the boundaries of the Antarctic continent (Ball, 1956). Nevertheless, even over vast ice sheets where the strongest terrestrial katabatic winds occur, the influence of large-scale pressure gradients and cloud cover cannot be neglected: the prediction of such events remains challenging even with state-of-the-art mesoscale models (Parish and Bromwich, 2007).

2.3. Martian examples

As favourable conditions for katabatic winds include terrain sloping over a large area, near-surface temperature inversions caused by nighttime radiative cooling and weak ambient winds, the fact that the Martian environment is conducive to such winds has been acknowledged before in situ missions were ever sent to Mars (Gierasch and Sagan, 1971). The short radiative timescales and low thermal inertia of the thin CO_2 Martian atmosphere account for katabatic winds two to three times stronger than on Earth (Blumsack et al., 1973). These estimates based on radiative relaxation time considerations can also be illustrated by calculating through Eq. (2) the ratio of "slope-buoyancy" Γ on the two
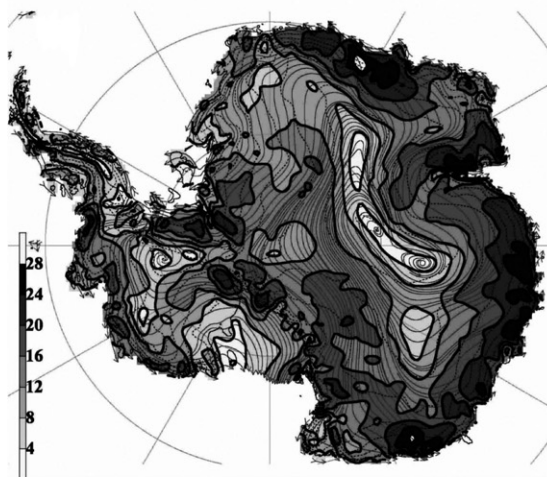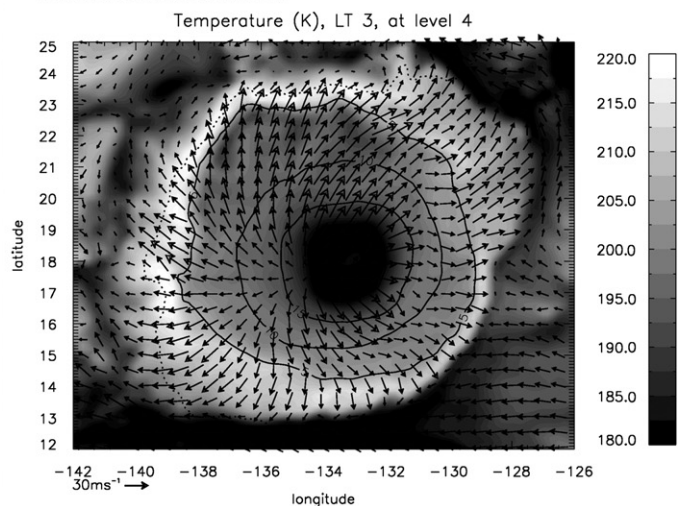
Fig. 2. Two examples of high-amplitude katabatic flow on the Earth over the Antarctic continent and on Mars over the Olympus Mons giant volcano. On the left, figure by Parish and Bromwich (2007) showing mean wind speed ($\mathrm{m\,s^{-1}}$) and streamlines over Antarctica approximately 100 m above the surface for the wintertime period. On the right, figure by Spiga and Forget (2009) showing nighttime downslope winds during northern fall approximately 120 m above the surface. Horizontal wind vectors are superimposed on the atmospheric temperature field. Maximum horizontal wind velocity is $\sim 40\,\mathrm{m\,s^{-1}}$ (reached close to Olympus caldera). Note the strong compressional heating caused by the winds at the base of the volcano.

planets over a slope of given inclination α in nighttime winter arid conditions.[6] Although the Martian gravity is three times smaller than its terrestrial counterpart, the downslope acceleration is three times larger owing to the colder environment and the much stronger nighttime inversions (the low-density Martian atmosphere yields shorter radiative timescales, see e.g. Goody and Belton, 1967).

Thus, as for katabatic winds, Mars might be regarded as an analog of terrestrial Antarctica in situation of clear skies (Parish and Bromwich, 2007): in both environments, dominant radiative control leads to strong near-surface temperature inversions (over 20 K) and clear-cut katabatic winds. Two notable differences can be mentioned. (1) On Mars the atmosphere is heated by strong absorption of incoming solar radiation in visible wavelengths by airborne dust. Changes in atmospheric dust loading impact both local thermal contrasts and static stability: Haberle et al. (1993a,b) suggested that near-surface slope winds are weaker when atmosphere is dustier (which acts as a negative feedback on dust lifting). (2) From the work by Mahrt and Larsen (1990), one could expect that the strong nighttime stability in the Martian environment ensures the predominance of katabatic flow over (possibly significant) ambient winds. Moreover, the daily temperature variations three times larger than on Earth (Hess et al., 1977), as well as the frequent absence of clouds, cause rapid transition from afternoon superadiabatic gradients to nighttime super-stable inversion, thus rapid onset of the katabatic wind regime.

Although very strong thermal winds (e.g. at the edge of the seasonal polar caps) were shown to alter the intensity of the katabatic winds (Siili et al., 1999), Martian mesoscale modeling confirmed that, in contrast to the terrestrial environment, katabatic winds are generally the most dominant source of mesoscale variability in nighttime conditions. All models available so far (see Introduction for a list of references) showed that, at various seasons and locations in the vicinity of craters and mountains, near-surface katabatic acceleration is repetitively predominant over background winds imposed by large-scale pressure gradients. This is particularly true in the vicinity of the giant topographic obstacles encountered on Mars: simulations of the Valles Marineris canyon by Richardson et al. (2007) without large-scale forcing yielded similar quantitative results for the near-surface wind speeds (over $5 \, \text{m s}^{-1}$ in the vertical and over $30 \, \text{m s}^{-1}$ in the horizontal) as other studies including the influence of ambient winds (Tyler et al., 2002; Toigo and Richardson, 2003; Rafkin and Michaels, 2003; Spiga and Forget, 2009). In such simulations, local maxima of vertical velocity correlate with topographic gradients (Spiga and Forget, 2009, Fig. 5). Intense katabatic flow is also predicted over Olympus Mons (Fig. 2). Spiga and Forget (2009) identified a persistent nighttime surface temperature enhancement at the base of the volcano (up to +20 K) which results from adiabatic compression of air masses by katabatic winds, similarly to what Nylen et al. (2004) noticed in Antarctica measurements. Note that polar regions on Mars are also conducive to strong katabatic winds (Kauhanen et al., 2008), owing to topographical gradients and ice coverage of the caps, but contrary to Earth it is not necessarily the location on the planet where those events are the most intense.

Numerical modeling studies show that clear-cut katabatic events are expected to be widespread on Mars and easier to detect than on Earth. Geological features (dunes or streaks) are thought to provide indirect evidence of repetitive nighttime katabatic inflow into craters, in good agreement with mesoscale model predictions (Greeley et al., 2003). Nighttime water ice cloud cover in areas of complex topography (e.g. Tharsis plateaus, see Wilson et al., 2007) is consistent between observations and mesoscale models, the latter showing dominant influence of katabatic winds in cloud formation (Spiga and Forget, 2009). Unfortunately, quantitative measurements of katabatic winds are seldom available and remain highly desirable in upcoming missions. Near-surface wind acquisitions to date were carried out on relatively flat terrains where it is difficult, though not impossible as shown e.g. by Leovy (1985) with Viking Landers (VL) and by Taylor et al. (2008) through the "telltale" experiment onboard Phoenix, to separate the katabatic circulation caused by large-scale slopes from other contributions. Savijärvi and Siili (1993) showed through idealised two-dimensional mesoscale simulations that stronger large-scale forcings at the low-latitude VL1 site reverse the diurnal turning of winds into backing, while at the higher latitude VL2 site with lower large-scale contribution, the combination of Coriolis and slope accelerations leads to direct veering throughout the day. The fact that katabatic circulation over moderate Martian slopes is constrained by large-scale circulation, notably thermal tides, is further supported by high-resolution general circulation modeling (S.R. Lewis, personal communication) and three-dimensional mesoscale simulations (Toigo and Richardson, 2002). Wind measurements in uneven topographical areas on Mars would be useful to unambiguously detect repetitive, intense, clear-cut katabatic events. At the same time, given the aforementioned difficulties encountered on Earth, those measurements would benefit to mesoscale meteorology in general.

3. Boundary layer convection

3.1. Preliminary comments

Turbulent convection in the daytime boundary layer originates from the influence of sun-heated ground on the first levels of the atmosphere (Stull, 1988). Numerous studies of convective processes in the terrestrial boundary layer have been carried out since the pioneering modeling work by Lilly (1962), completing the in situ observational approach that prevailed beforehand. Spatial exploration of Mars showed the intensity of Martian boundary layer processes, driven by large diurnal surface temperature variations (Gierasch and Goody, 1968): convective heat flux three times larger than in the terrestrial environment (Sutton et al., 1978), wide dust devils with high altitude extent (Malin and Edgett, 2001) and strong daytime super-adiabatic near-surface gradients of temperature ($5–10 \, \text{K m}^{-1}$) (Schofield et al., 1997).

Parameterised single-column models were employed to interpret in situ measurements and clarified the role of radiation in the Martian boundary layer energy budget (Haberle et al., 1993a,b; Sävijarvi, 1999). Tillman et al. (1994) and Larsen et al. (2002) found that the behaviour of surface layer turbulence and mean flow on Mars obeys the same scaling laws as on Earth; thus differences mainly arise from the low density of the Martian atmosphere. Scaling theory initially developed to explain terrestrial dust devils yields correct estimates for dust devils observed on Mars (Renno et al., 2000). Since the beginning of the 2000s, the dynamics of the Martian convective boundary layer is analysed by means of large eddy simulations (Rafkin et al., 2001; Toigo et al., 2003; Michaels and Rafkin, 2004; Tyler et al., 2008), where grid spacing in Martian mesoscale models is lowered to a few tens of metres so as to resolve the larger turbulent eddies, responsible for

---

[6] Earth (typical radiosounding profile): Tamanrasset in Sahara desert, 22.8N, 5.43E, local time is midnight, $\langle T \rangle = 285 \, \text{K}$, $\Delta T = 5 \, \text{K}$ between 0 and 250 m above the surface, $g = 9.81 \, \text{m s}^{-2}$; Mars (extract from the European Mars Climate Database): same coordinates, same local time, $\langle T \rangle = 175 \, \text{K}$, $\Delta T = 30 \, \text{K}$ between 0 and 250 m above the surface, $g = 3.72 \, \text{m s}^{-2}$.

most of the energy transport within the convective boundary layer.

This "chronological" perspective—from 1D to 3D models—is adopted in what follows: the vertical thermal structure and energy budget in the boundary layer both on Mars and on the Earth are discussed, before consequences on the convective dynamics are examined.

3.2. Energy budget in the Martian and terrestrial boundary layers

What is the energy budget in daytime conditions a few 10 s metres above the surface[7] both on Mars and the Earth? Without losing generality, four contributions to the total atmospheric heating rate $\mathcal{J}$ can be listed[8]:(1) the sensible heat flux $\mathcal{J}_S$, i.e. heat transfer between the surface and the atmosphere by conduction and convection, (2) the condensation or evaporation energy transfers $\mathcal{J}_{LH}$, (3) the convergence of net infrared radiative flux $\mathcal{J}_{LW}$, (4) the convergence of net shortwave radiative flux $\mathcal{J}_{SW}$.

On Earth, the two dominant terms are the sensible heat flux $\mathcal{J}_S$ (very prominent, e.g. 20% of the incoming solar flux in terrestrial deserts) and the latent component $\mathcal{J}_{LH}$ (of importance outside arid regions). In contrast to these two terms, radiative contributions in the infrared $\mathcal{J}_{LW}$ and in the visible $\mathcal{J}_{SW}$ are negligible. Only in very peculiar meteorological and surface conditions of high-elevation sites (e.g. the Tibetan Plateaus on clear days), the radiative contribution can be significant (Smith and Shi, 1992).

The two dominant contributions to the energy budget of terrestrial daytime near-surface atmosphere have less impact on Mars. Owing to low atmospheric density and thermal inertia, the sensible contribution $\mathcal{J}_S$ is only 2% of the incoming solar flux (Sutton et al., 1978). Mars is a dry planet: although relative humidity is often close to 100% and leads to the formation of clouds and fog in the boundary layer (Whiteway et al., 2009), low values of Martian specific humidity cause $\mathcal{J}_{LH}(H_2O)$ to be negligible (Sävijarvi, 1999). The main atmospheric component CO_2 undergoes condensation/sublimation, but low transition temperature implies that $\mathcal{J}_{LH}(CO_2)$ is negligible outside polar regions.

Major contributors to the total heating rate $\mathcal{J}$ are, in contrast to the terrestrial environment, the radiative terms $\mathcal{J}_{LW}$ and $\mathcal{J}_{SW}$. This is a consequence of the predominance of CO_2 and dust in the tenuous Martian atmosphere. Upwelling thermal infrared radiation from the insolated soil is prone to strong net absorption by the colder atmospheric CO_2 and, to lesser extent, H_2O and dust (Sävijarvi, 1999). Up to several 100 s of metres above ground, from

mid-morning to late afternoon, the infrared term $\mathcal{J}_{LW}$ dominates the boundary layer energy budget (Haberle et al., 1993a, b). Only in very dusty conditions, direct absorption of incoming solar radiation in the visible by airborne dust $\mathcal{J}_{SW}$ significantly contributes to the total heating rate.

The dominant driver of daytime boundary layer dynamics is to first order the sensible term $\mathcal{J}_S$ in terrestrial arid regions and the infrared radiative term $\mathcal{J}_{LW}$ in the Martian environment (although the sensible contribution $\mathcal{J}_S$ cannot be neglected). In both cases, the key parameter influencing lower atmospheric temperatures is surface temperature (controlled by insolation, soil properties and elevation) but near-surface Martian and terrestrial thermal structures differ. Contrary to the denser terrestrial environment, the influence of sensible and latent heat fluxes on the Martian soil energy budget is negligible: surface is close to radiative equilibrium and its temperature does not vary much with topography. Infrared heating rate $\mathcal{J}_{LW}$ (and, to first order, total heating rate $\mathcal{J}$) is also fairly independent of altimetry, for variations of the absorbed radiative energy in the infrared with pressure are negligible in the thin Martian near-surface CO_2 atmosphere (Goody and Belton, 1967).

Thus, near-surface Martian atmospheric isotherms adopt a terrain-following behaviour,[9] not observed on Earth where daytime surface and lower atmospheric temperatures are colder over mountains than in lower plains. As detailed in Spiga et al. (2010), this radiatively controlled thermal structure of the Martian boundary layer and the associated positive correlations between boundary layer depth and surface altimetry are confirmed through Mars Express radio-occultation measurements Hinson et al. (2008).

3.3. Boundary layer dynamics

Characteristics of boundary layer dynamics on both planets are discussed here through Large Eddy Simulations (free convection typical cases with no background winds). A reference terrestrial case study of dry convection over land is the well-known Wangara dataset over an "ideal" flat, homogeneous Australian site devoid of topographical forcings (Hess et al., 1981), which has been widely referred to for validation of turbulence closure models (Yamada and Mellor, 1975). Recent results obtained through 30-m horizontal resolution large eddy simulations by Basu et al. (2008) are used as a reference. The simulations were performed on summertime, with clear conditions, nearly no horizontal advection of heat or moisture and lack of any frontal activity within 1000 km. Results are in agreement with in situ measurements and independent modeling.

Martian large-eddy simulations performed at 50 m horizontal resolution with the model described in Spiga and Forget (2009) for two typical cases in spring (Amazonis low plains and Tharsis high plateaus) are compared to Basu et al. (2008) terrestrial simulations. Use of the Martian Mesoscale Model by Spiga and Forget (2009) in large eddy simulations yields consistent results compared to other models (Michaels and Rafkin, 2004; Toigo et al., 2003; Sorbjan, 2007; Richardson et al., 2007). Detailed description of simulations can be found in Spiga et al. (2010), where it is shown that the predicted boundary layer depth and mixing layer potential temperature are in agreement with remote-sensing retrievals (Hinson et al., 2008).

Daytime growths of terrestrial and Martian convective boundary layers are shown in Fig. 3 by means of horizontal and vertical velocity variances and vertical eddy heat fluxes (Stull, 1988).

---

[7] That is, at the bottom of the mixed-layer, or equivalently at the top of the surface layer.

[8] The contribution of sensible heat flux is referred to as a heating rate, though it has a slightly different nature than the other terms (for it is itself related to boundary layer turbulence). As it is described in greater detail in Spiga et al. (2010), the law of evolution of mixed-layer potential temperature θ in daytime conditions reads

$$c_p \frac{\partial \theta}{\partial t} = \left(\frac{p_0}{p}\right)^{R/c_p} (\mathcal{J}_{LH} + \mathcal{J}_{LW} + \mathcal{J}_{SW}) - c_p \frac{\partial \langle w'\theta' \rangle}{\partial z}$$

with specific heat capacity c_p, atmospheric pressure p, reference pressure p_0, gas constant R, vertical velocity w, turbulent component $\cdot'$. At the bottom of the mixed layer, i.e. at a small distance dz above the surface layer top, the rightmost term writes $\rho c_p \, d \langle w'\theta' \rangle \approx \rho c_p \langle w'\theta' \rangle_z - H_s$ (where ρ is the atmospheric density and H_s is the effective sensible heat flux), i.e. combination of molecular transfer from heated surface in the microlayer and small-scale turbulent transport in the surface layer. For the sake of conciseness, discussions in the present paper make use of an equivalent sensible heating rate $\mathcal{J}_S$ defined as

$$\mathcal{J}_S = -\left(\frac{p}{p_0}\right)^{R/c_p} c_p \frac{\partial \langle w'\theta' \rangle}{\partial z}.$$
.

[9] The fact that sensible heat flux $\mathcal{J}_S$ is not negligible results in isotherms being comparatively closer to the ground at higher surface elevation.
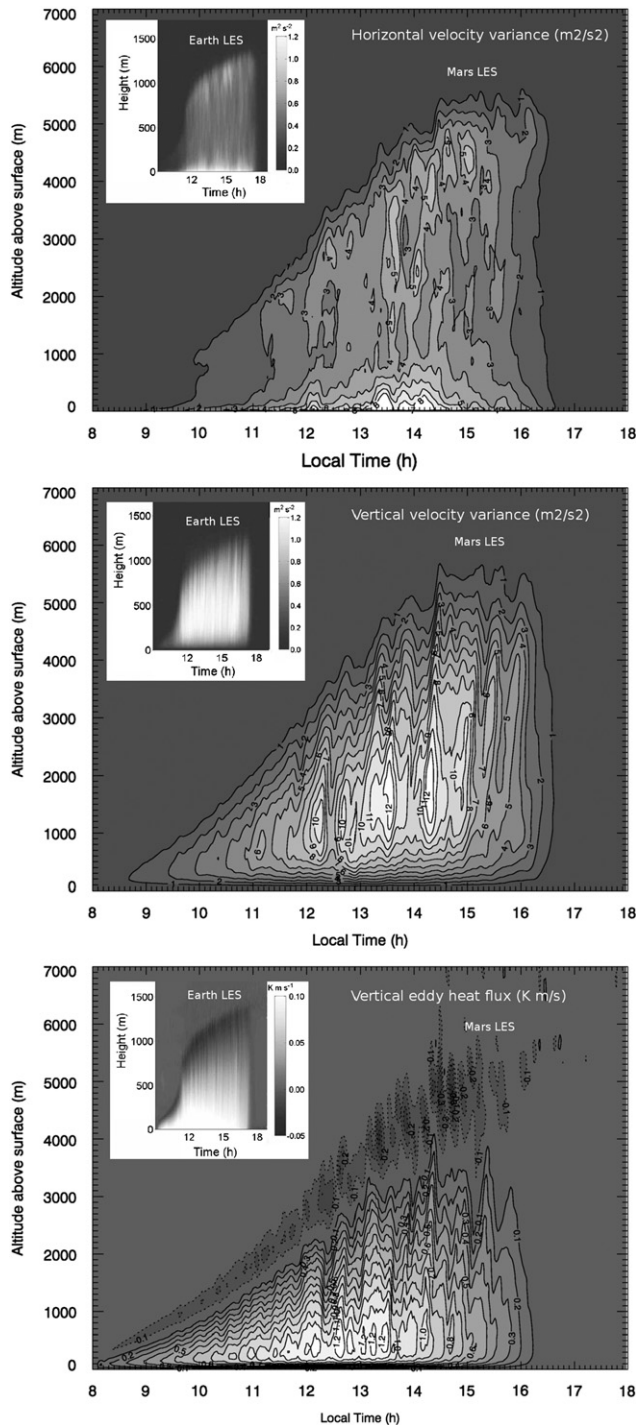
Fig. 3. Evolution of daytime convective boundary layer statistics: time-height plots of the modeled-resolved horizontal velocity variance (top), vertical velocity variance (middle) and vertical eddy heat flux (bottom). Results from large-eddy simulations of a typical Martian spring case in the Amazonis Planitia plains by Spiga et al. (2010) and of the terrestrial Wangara reference summertime case by Basu et al. (2008) are shown. Perturbations X' of a given field X are calculated by subtracting from the total field an average field $\langle X \rangle$ obtained by temporal smoothing with a window of 200 s for the Martian case. Note that displayed horizontal velocity variance is $\langle u'^2 \rangle$; evolution of the other horizontal component $\langle v'^2 \rangle$, not shown, is similar.

Large-eddy simulations confirm what was first shown by single-column studies: convective boundary layer on Mars may reach considerable depth (e.g. 5 km in Amazonis low plains, as shown in Fig. 3, and 8 km in Tharsis high plateaus) while terrestrial values are moderate (1.4 km in the Wangara case, sometimes extreme values of 4–5 km are observed in hot arid deserts). The overall evolution of horizontal and vertical velocity variances are similar on the two planets, but Martian boundary layer turbulence is one order of magnitude more vigorous than its terrestrial counterpart. While velocity variances reach $1.2\,m^2\,s^{-2}$ on Earth (near the surface for the horizontal component and 300–500 m above the ground for the vertical component), maximum values on Mars are, respectively, $8\,m^2\,s^{-2}$ near the surface and $12\,m^2\,s^{-2}$ within the convective boundary layer. Unlike the terrestrial case, the Martian vertical variance is nearly twice the horizontal value (except close to the surface and the boundary layer top). The total turbulent kinetic energy for this particular case reaches $10\,m^2\,s^{-2}$, to be compared to the Wangara experiment value of $1.1\,m^2\,s^{-2}$. Note that the Amazonis case features a 5 km-deep convective boundary layer, which is "low" to Martian standards out of high-latitude regions. In the more extreme case of the Tharsis high plateaus (5 km depth), turbulent kinetic energy of $\sim 18\,m^2\,s^{-2}$ is predicted: comparison of the two Martian cases illustrates the large regional variability of the Martian boundary layer dynamics (Spiga et al., 2010).

Values of vertical eddy heat flux are an order of magnitude higher in the tenuous Martian environment (-0.3 to $1.2\,K\,m\,s^{-1}$) than on Earth (-0.05 to $0.1\,K\,m\,s^{-1}$). The "low plains" Martian case exhibits stronger heat flux than the "high plateaus" Tharsis case (approximately a factor of 2). This results from strong radiative control exerted on the Martian daytime boundary layer, because heat flux and inverse near-surface pressure are expected to be correlated, for the heating rate is fairly independent of elevation (Spiga et al., 2010 and Section 3.2 of this paper).

Another notable consequence of the Martian radiative control, shown in Fig. 3, is that the turbulent heat flux is not maximum near the surface, as is the case on Earth, but a few hundreds of metres above the surface (Savijarvi, 1991; Michaels and Rafkin, 2004). Decreasing (increasing) heat flux with altitude indicates warming (cooling) by boundary layer convection. Martian radiative infrared heating is so strong in the lowest atmospheric levels that near-surface convective processes act to cool the atmosphere rather than warm it, which agrees with earlier diagnostics from single-column models (Haberle et al., 1993a, b; Savijärvi et al., 2004).

Mars confirms that boundary layer has to be defined as the part of the atmosphere influenced by the *presence* of the surface, and not only by the surface itself. On Earth the afternoon boundary layer warms "from below" by sensible heat flux incoming from the heated surface, whereas on Mars it warms "from inside and from below", respectively, by infrared radiative heating (plus the visible absorption by the dust) and sensible heat flux. In the Martian environment, the energy that fuels the thermals of mean typical velocity w_* does not originate only from the atmospheric levels immediately close to the surface. Thus, a version of mixing layer formulae valid both on Mars and on Earth should substitute the maximum heat flux $\langle w'\theta' \rangle_{max}$ for the surface heat flux $\langle w'\theta' \rangle_0$. For instance, only the relationship[10]

$$w_* = \left[gz_i \frac{\langle w'\theta' \rangle_{max}}{\langle \theta \rangle} \right]^{1/3} \tag{3}$$

enables one to calculate Martian vertical velocity scale w_* consistent with resolved convective motions by large-eddy simulations. Values of $w_* = 4$–$6.5\,m\,s^{-1}$ obtained for Mars account for the vigorous convection compared to Earth ($w_* < 2\,m\,s^{-1}$), in good agreement with similarity estimates based on observations (Sutton et al., 1978; Martínez et al., 2009).

---

[10] z_i is the boundary layer depth and θ is the potential temperature.

4. Conclusive remarks

The main conclusions of the paper are summarised in the abstract and are not reproduced here for the sake of brevity. It is hoped that the comparative discussion on two specific mesoscale phenomena in this paper will be followed by increasingly comprehensive reviews in the future. Although elements of comparison between Mars and the Earth can already be put into perspective, the Martian mesoscale variability remains to be explored in greater detail, especially with additional measurements of wind and temperature, in order to validate diagnostics derived from numerical models and to expand the knowledge of mesoscale phenomena by new case studies in extreme environments. So far, observations of Martian phenomena have not altered the theoretical background through which the mesoscale terrestrial phenomena can be described. Analysis of "exotic" mesoscale processes on Mars might help to further test this theoretical background: for instance, detection of CO_2 clouds of possible convective origin in the Martian high altitudes (60–90 km), where atmospheric density is extremely low, raises fundamental questions about deep convection processes (Montmessin et al., 2007).

Mars is not the only extraterrestrial planet on which mesoscale phenomena have been observed and modeled. Convective clouds of methane on Titan (Barth and Rafkin, 2007), of water on Jupiter (Hueso and Sánchez-Lavega, 2001), of sulfuric acid on Venus (Russell et al., 2006) have recently been examined through idealised mesoscale simulations. Gravity waves have also been identified on Venus (Peralta et al., 2008) and on giant planets (Reuter et al., 2007). Deep convection and gravity waves are two crucial phenomena known to influence the large-scale circulation (Fritts and Alexander, 2003; Li et al., 2006). Thus, studying and comparing mesoscale phenomena in various planetary environments may give insights not only into the general principles of mesoscale meteorology, but into key phenomena influencing the global climate too.

Acknowledgment

References

Anthes, R.A., Rosenthal, S.L., Trout, J.W., 1971. Preliminary results from an asymmetric model of the tropical cyclone. Monthly Weather Review 99 (10), 744–758.

Ball, F., 1956. The theory of strong Katabatic winds. Australian Journal of Physics 9, 373.

Barth, E., Rafkin, S., 2007. TRAMS: a new dynamic cloud model for Titan's methane clouds. Geophysical Research Letters 34, L03203.

Basu, S., Vinuesa, J.-F., Swift, A., 2008. Dynamic LES modeling of a diurnal cycle. Journal of Applied Meteorology and Climatology 47, 1156–+.

Blumsack, S.L., Gierasch, P.J., Wessel, W.R., 1973. An analytical and numerical study of the Martian planetary boundary layer over slopes. Journal of Atmospheric Sciences 30, 66–82.

Bromwich, D.H., Cassano, J.J., Klein, T., Heinemann, G., Hines, K.M., Steffen, K., Box, J.E., 2001. Mesoscale modeling of Katabatic winds over Greenland with the Polar MM5. Monthly Weather Review 129, 2290–+.

Creasey, J.E., Forbes, J.M., Hinson, D.P., 2006. Global and seasonal distribution of gravity wave activity in Mars' lower atmosphere derived from MGS radio occultation data. Geophysical Research Letters 33, 1803.

Davy, R., Davis, J.A., Taylor, P.A., Lange, C.F., Weng, W., Whiteway, J., Gunnlaugson, H.P., 2010. Initial analysis of air temperature and related data from the Phoenix MET station and their use in estimating turbulent heat fluxes. Journal of Geophysical Research (Planets) 115 (E14), 0–+.

Doran, J.C., Horst, T.W., Whiteman, C.D., 1990. The development and structure of nocturnal slope winds in a simple valley. Boundary-Layer Meteorology 52, 41–68.

Drobinski, P., Haeberli, C., Richard, E., Lothon, M., Dabas, A.M., Flamant, P.H., Furger, M., Steinacker, R., 2003. Scale interaction processes during the MAP IOP 12 south foehn event in the Rhine Valley. Quarterly Journal of the Royal Meteorological Society 129, 729–753.

Fedorovich, E., Rotunno, R., Stevens, B., 2004. Atmospheric Turbulence and Mesoscale Meteorology. Cambridge University Press, Cambridge.

Forget, F., Hourdin, F., Fournier, R., Hourdin, C., Talagrand, O., Collins, M., Lewis, S.R., Read, P.L., Huot, J.-P., 1999. Improved general circulation models of the Martian atmosphere from the surface to above 80 km. Journal of Geophysical Research 104 (24), 24,155–24,176.

Fritts, D., Alexander, M., 2003. Gravity wave dynamics and effects in the middle atmosphere. Reviews of Geophysics 41 (1), 1003.

Gierasch, P., Sagan, C., 1971. A preliminary assessment of Martian wind regimes. Icarus 14, 312–+.

Gierasch, P.J., Goody, R.M., 1968. A study of the thermal and dynamical structure of the Martian lower atmosphere. Planetary and Space Science 16, 615–646.

Goody, R., Belton, M.J.S., 1967. Radiative relaxation times for Mars. A discussion of martian atmospheric dynamics. Planetary and Space Science 15, 247–+.

Greeley, R., Kuzmin, R.O., Rafkin, S.C.R., Michaels, T.I., Haberle, R., 2003. Wind-related features in Gusev crater, Mars. Journal of Geophysical Research (Planets) 108, 8077–+.

Haberle, R., Houben, H.C., Hertenstein, R., Herdtle, T., 1993a. A boundary layer model for Mars: comparison with Viking Lander and entry data. Journal of the Atmospheric Sciences 50, 1544–1559.

Haberle, R.M., Pollack, J.B., Barnes, J.R., Zurek, R.W., Leovy, C.B., Murphy, J.R., Lee, H., Schaeffer, J., 1993b. Mars atmospheric dynamics as simulated by the NASA/Ames general circulation model, 1, the zonal-mean circulation. Journal of Geophysical Research 98 (E2), 3093–3124.

Hess, G.D., Hicks, B.B., Yamada, T., 1981. The impact of the Wangara experiment. Boundary-Layer Meteorology 20, 135–174.

Hess, S.L., Henry, R.M., Leovy, C.B., Ryan, J.A., Tillman, J.E., 1977. Meteorological results from the surface of Mars: viking 1 and 2. Journal of Geophysical Research 82, 4559–4574.

Hinson, D.P., Pätzold, M., Tellmann, S., Häusler, B., Tyler, G.L., 2008. The depth of the convective boundary layer on Mars. Icarus 198, 57–66.

Horst, T.W., Doran, J.C., 1986. Nocturnal drainage flow on simple slopes. Boundary-Layer Meteorology 34, 263–286.

Hueso, R., Sánchez-Lavega, A., 2001. A three-dimensional model of moist convection for the giant planets: the Jupiter case. Icarus 151, 257–274.

Kauhanen, J., Siili, T., Järvenoja, S., Savijärvi, H., 2008. The Mars limited area model and simulations of atmospheric circulations for the Phoenix landing area and season of operation. Journal of Geophysical Research (Planets) 113 (E12), 0–+.

Larsen, S.E., Jørgensen, H.E., Landberg, L., et al., 2002. Aspects of the atmospheric surface layers on Mars and Earth. Boundary-Layer Meteorology 105, 451–470.

Leovy, C., 1985. The general circulation of Mars: model and observations. Advance in Geophysics 28a, 327–346.

Li, L., Ingersoll, A.P., Huang, X., 2006. Interaction of moist convection with zonal jets on Jupiter and Saturn. Icarus 180, 113–123.

Lilly, D., Kennedy, P., 1973. Observations of a stationary mountain wave and its associated momentum flux and energy dissipation. Journal of the Atmospheric Sciences 30 (6), 1135–1152.

Lilly, D.K., 1962. On the numerical simulation of buoyant convection. Tellus 14 (2), 148–172.

Mahrer, Y., Pielke, R., 1977. The effects of topography on sea and land breezes in a two-dimensional numerical model. Monthly Weather Review 105 (9), 1151–1162.

Mahrt, L., 1982. Momentum balance of gravity flows. Journal of the Atmospheric Sciences 39 (12), 2701–2711.

Mahrt, L., Larsen, S., 1990. Relation of slope winds to the ambient flow over gentle terrain. Boundary-Layer Meteorology 53, 93–102.

Malin, M.C., Calvin, W.M., Cantor, B.A., Clancy, R.T., Haberle, R.M., James, P.B., Thomas, P.C., Wolff, M.J., Bell, J.F., Lee, S.W., 2008. Climate, weather, and north polar observations from the Mars Reconnaissance Orbiter Mars Color Imager. Icarus 194, 501–512.

Malin, M.C., Edgett, K.S., 2001. Mars Global Surveyor Mars Orbiter Camera: interplanetary cruise through primary mission. Journal of Geophysical Research 106, 23429–23570.

Manins, P., Sawford, B., 1979. A model of Katabatic winds. Journal of the Atmospheric Sciences 36 (4), 619–630.

Martínez, G., Valero, F., Vázquez, L., 2009. Characterization of the Martian convective boundary layer. Journal of Atmospheric Sciences 66, 2044–2058.

Michaels, T.I., Colaprate, A., Rafkin, S.C.R., 2006. Significant vertical water transport by mountain-induced circulations on Mars. Geophysical Research Letters 33, 16201.

Michaels, T.I., Rafkin, S.C.R., 2004. Large eddy simulation of atmospheric convection on Mars. Quarterly Journal of the Royal Meteorological Society 128.

Montmessin, F., Gondet, B., Bibring, J.-P., Langevin, Y., Drossart, P., Forget, F., Fouchet, T., 2007. Hyperspectral imaging of convective CO_2 ice clouds in the equatorial mesosphere of Mars. Journal of Geophysical Research (Planets) 112, 11–+.

Nylen, T.H., Fountain, A.G., Doran, P.T., 2004. Climatology of katabatic winds in the McMurdo dry valleys southern Victoria Land, Antarctica. Journal of Geophysical Research (Atmospheres) 109, 3114–+.

Orlanski, I., 1975. A rational subdivision of scales for atmospheric processes. Bulletin of the American Meteorological Society 56 (5), 527–534.

Papadopoulos, K., Helmis, C., 1999. Evening and morning transition of katabatic flows. Boundary-Layer Meteorology 92 (2), 195–227.

Parish, T.R., 2003. Katabatic winds. In: Holton, J.R., Pyle, J., Curry, J.A. (Eds.), Encyclopedia of Atmospheric Sciences.

Parish, T.R., Bromwich, D.H., 2007. Reexamination of the near-surface airflow over the Antarctic continent and implications on atmospheric circulations at high southern latitudes*. Monthly Weather Review 135, 1961–+.

Parish, T.R., Waight, K.T., 1987. The forcing of Antarctic Katabatic winds. Monthly Weather Review 115, 2214–+.

Parmhed, O., Oerlemans, J., Grisogono, B., 2004. Describing surface fluxes in katabatic flow on Breidamerkurjökull, Iceland. Quarterly Journal of the Royal Meteorological Society 130, 1137–1151.

Peralta, J., Hueso, R., Sánchez-Lavega, A., Piccioni, G., Lanciano, O., Drossart, P., 2008. Characterization of mesoscale gravity waves in the upper and lower clouds of Venus from VEX-VIRTIS images. Journal of Geophysical Research (Planets) 113, 0–+.

Pickersgill, A.O., Hunt, G.E., 1979. The formation of Martian lee waves generated by a crater. Journal of Geophysical Research 84 (B14), 8317–8331.

Pielke, R., Cotton, W., Walko, R., Trembaek, C., Lyons, W., Grasso, L., Nieholls, M., Moran, M., Wesley, D., Lee, T., et al., 1992. A comprehensive meteorological modeling system-RAMS. Meteorology and Atmospheric Physics 49, 69–91.

Rafkin, S.C.R., Haberle, R.M., Michaels, T.I., 2001. The Mars regional atmospheric modeling system: model description and selected simulations. Icarus 151, 228–256.

Rafkin, S.C.R., Michaels, T.I., 2003. Meteorological predictions for 2003 Mars Exploration Rover high-priority landing sites. Journal of Geophysical Research 108 (E12) 8091–+.

Rafkin, S.C.R., Sta. Maria, M.R.V., Michaels, T.I., 2002. Simulation of the atmospheric thermal circulation of a martian volcano using a mesoscale numerical model. Nature 419, 697–699.

Renno, N.O., Nash, A.A., Lunine, J., Murphy, J., 2000. Martian and terrestrial dust devils: test of a scaling theory using Pathfinder data. Journal of Geophysical Research 105, 1859–1866.

Reuter, D., Simon-Miller, A., Lunsford, A., Baines, K., Cheng, A., Jennings, D., Olkin, C., Spencer, J., Stern, S., Weaver, H., et al., 2007. Jupiter cloud composition, stratification, convection, and wave motion: a view from new horizons. Science 318 (5848), 223.

Richardson, M.I., Toigo, A.D., Newman, C.E., 2007. PlanetWRF: a general purpose local to global numerical model for planetary atmospheric and climate dynamics. Journal of Geophysical Research 112 (E09001).

Russell, C.T., Strangeway, R.J., Zhang, T.L., 2006. Lightning detection on the Venus Express mission. Planetary and Space Science 54, 1344–1351.

Savijarvi, H., 1991. A model study of the PBL structure on Mars and the earth. Contributions to Atmospheric Physics/Beitraege zur Physik Atmosphaere 64, 219–229.

Sävijarvi, H., 1999. A model study of the atmospheric boundary layer in the Mars Pathfinder lander conditions. Quarterly Journal of the Royal Meteorological Society 125 (554), 483–493.

Savijärvi, H., Määttänen, A., Kauhanen, J., Harri, A.-M., 2004. Mars pathfinder: new data and new model simulations. Quarterly Journal of the Royal Meteorological Society 130, 669–683.

Savijärvi, H., Siili, T., 1993. The Martian slope and the nocturnal PBL jet. Journal of the Atmospheric Sciences 50, 77–88.

Schofield, J.T., Crisp, D., Barnes, J.R., Haberle, R.M., Magalhaães, J.A., Murphy, J.R., Seiff, A., Larsen, S., Wilson, G., 1997. The Mars Pathfinder Atmospheric Structure Investigation/Meteorology (ASI/MET)experiment. Science 278, 1752–1757.

Siili, T., Haberle, R.M., Murphy, J.R., Savijarvi, H., 1999. Modelling of the combined late-winter ice cap edge and slope winds in Mars Hellas and Argyre regions. Planetary and Space Science 47, 951–970.

Skamarock, W.C., Klemp, J.B., 2008. A time-split nonhydrostatic atmospheric model for weather research and forecasting applications. Journal of Computational Physics 227, 3465–3485.

Skyllingstad, E.D., 2003. Large-eddy simulation of Katabatic flows. Boundary-Layer Meteorology 106, 217–243.

Smith, E., Shi, L., 1992. Surface forcing of the infrared cooling profile over the Tibetan plateau. Part I: influence of relative longwave radiative heating at high altitude. Journal of the Atmospheric Sciences 49 (10), 805–822.

Smith, M.D., Wolff, M.J., Spanovich, N., Ghosh, A., Banfield, D., Christensen, P.R., Landis, G.A., Squyres, S.W., 2006. One Martian year of atmospheric observations using MER Mini-TES. Journal of Geophysical Research (Planets) 111 (E10), 12–+.

Sorbjan, Z., 2007. Statistics of shallow convection on Mars based on large-eddy simulations. Part 1: shearless conditions. Boundary-Layer Meteorology 123, 121–142.

Souza, E.P., Rennó, N.O., Silva Dias, M.A.F., 2000. Convective circulations induced by surface heterogeneities. Journal of Atmospheric Sciences 57, 2915–2922.

Spiga, A., Forget, F., 2009. A new model to simulate the Martian mesoscale and microscale atmospheric circulation: validation and first results. Journal of Geophysical Research (Planets) 114 (E13), 2009–+.

Spiga, A., Forget, F., Dolla, B., Vinatier, S., Melchiorri, R., Drossart, P., Gendrin, A., Bibring, J.-P., Langevin, Y., Gondet, B., 2007. Remote sensing of surface pressure on Mars with the Mars Express/OMEGA spectrometer: 2. Meteorological maps. Journal of Geophysical Research Planets 112 (E11), 8–+.

Spiga, A., Forget, F., Lewis, S.R., Hinson, D.P., 2010. Structure and dynamics of the convective boundary layer on Mars as inferred from large-eddy simulations and remote-sensing measurements. Quarterly Journal of the Royal Meteorological Society 136, 414–428.

Stanzel, C., Pätzold, M., Williams, D.A., Whelley, P.L., Greeley, R., Neukum, G., 2008. The HRSC Co-Investigator Team, dust devil speeds, directions of motion and general characteristics observed by the Mars Express High Resolution Stereo Camera. Icarus 197, 39–51.

Stull, R.B., 1988. An Introduction to Boundary Layer Meteorology. Kluwer Academic Publishers.

Sutton, J.L., Leovy, C.B., Tillman, J.E., 1978. Diurnal variations of the Martian surface layer meteorological parameters during the first 45 sols at two Viking lander sites. Journal of the Atmospheric Sciences 35, 2346–2355.

Taylor, P.A., Gunnlaugsson, H.P., Holstein-Rathlou, C., Lange, C.F., Moores, J., Cook, C., Dickinson, C., Popovici, V., Seabrook, J., Whiteway, J., 2008. Phoenix: summer Weather in Green Valley (126W, 68N on Mars). LPI Contributions 1447, 9024–+.

Thomas, P., Gierasch, P.J., 1985. Dust devils on Mars. Science 230, 175–177.

Thorpe, A.J., Volkert, H., Ziemianski, M.J., 2003. The Bjerknes' circulation theorem: a historical perspective. Bulletin of the American Meteorological Society 84 (4), 471–480.

Tillman, J.E., Landberg, L., Larsen, S.E., 1994. The boundary layer of Mars: fluxes stability, turbulent spectra and growth of the mixed layer. Journal of the Atmospheric Sciences 51 (12), 1709–1727.

Toigo, A.D., Richardson, M.I., 2002. A mesoscale model for the Martian atmosphere. Journal of Geophysical Research (Planets) 107, 5049–+.

Toigo, A.D., Richardson, M.I., 2003. Meteorology of proposed Mars Exploration Rover landing sites. Journal of Geophysical Research 108 (E12) 8092–+.

Toigo, A.D., Richardson, M.I., Ewald, S.P., Gierasch, P.J., 2003. Numerical simulation of Martian dust devils. Journal of Geophysical Research (Planets), 108, 5047.

Tyler, D., Barnes, J.R., 2005. A mesoscale model study of summertime atmospheric circulations in the north polar region of Mars. Journal of Geophysical Research (Planets) 110 (E9), 6007–+.

Tyler, D., Barnes, J.R., Haberle, R.M., 2002. Simulation of surface meteorology at the Pathfinder and VL1 sites using a Mars mesoscale model. Journal of Geophysical Research (Planets) 107, 5018–+.

Tyler, D., Barnes, J.R., Skyllingstad, E.D., 2008. Mesoscale and large-eddy simulation model studies of the Martian atmosphere in support of Phoenix. Journal of Geophysical Research (Planets) 113 (E12), 0–+.

Wang, H., Ingersoll, A.P., 2002. Martian clouds observed by Mars Global Surveyor Mars Orbiter Camera. Journal of Geophysical Research 107, 5078–+.

Wang, H., Richardson, M.I., Wilson, R.J., Ingersoll, A.P., Toigo, A.D., Zurek, R.W., 2003. Cyclones, tides, and the origin of a cross-equatorial dust storm on Mars. Geophysical Research Letters 30, 1488.

Whiteman, C.D., Zhong, S., Bian, X., 1999. Wintertime Boundary Layer Structure in the Grand Canyon. Journal of Applied Meteorology 38, 1084–1102.

Whiteway, J.A., Komguem, L., Dickinson, C., Cook, C., Illnicki, M., Seabrook, J., Popovici, V., Duck, T.J., Davy, R., Taylor, P.A., Pathak, J., Fisher, D., Carswell, A.I., Daly, M., Hipkin, V., Zent, A.P., Hecht, M.H., Wood, S.E., Tamppari, L.K., Renno, N., Moores, J.E., Lemmon, M.T., Daerden, F., Smith, P.H., 2009. Mars water-ice clouds and precipitation. Science 325, 68––.

Wilson, R.J., Neumann, G.A., Smith, M.D., 2007. Diurnal variation and radiative influence of Martian water ice clouds. Geophysical Research Letters 34, 2710.

Yanai, M., 1961. A detailed analysis of typhoon formation. Journal of the Meteorological Society of Japan 39, 187–214.

Yamada, T., Mellor, G., 1975. A simulation of the Wangara atmospheric boundary layer data. Journal of Atmospheric Sciences 32, 2309.

Ye, Z.J., Segal, M., Pielke, R.A., 1990. A comparative study of daytime thermally induced upslope flow on Mars and Earth. Journal of Atmospheric Sciences 47, 612–628.